Electronic Supplementary Material (ESI) for Journal of Materials Chemistry A.

Support Information

Oxygen-deficient WO_{3-x}@TiO_{2-x} Core-Shell Nanosheets for Efficient Photoelectrochemical Oxidation of Neutral Water Solutions

Kaiping Yuan[a,b,c,&], Qi Cao[d,&], Hong-Liang Lu[a,c,*], Miao Zhong[e], Xiuzhen Zheng[f], Hong-Yan Chen[a,c], Tao Wang[a,c], Jean-Jacques Delaunay[d], Wei Luo[f], Liwu Zhang[g], Yuan-Yuan Wang[a,c], Yonghui Deng[h], Shi-Jin Ding[a,c] & David Wei Zhang[a,c,*]

[a] *State Key Laboratory of ASIC and System,* [b] *Department of Electronic Engineering,* [c] *School of Microelectronics, Fudan University, Shanghai 200433, China.* [d] *Department of Mechanical Engineering,* [e] *Department of Chemical System Engineering, The University of Tokyo, Hongo 7-3-1, Bunkyo-ku, Tokyo 113-8656, Japan.* [f] *State Key Laboratory for Modification of Chemical Fibers and Polymer Materials, College of Materials Science and Engineering, Donghua University, Shanghai 201620, China* [g] *Department of Environmental Science and Engineering, Fudan University, Shanghai 200433, China.* [h] *Department of Chemistry, Fudan University, Shanghai 200433, China.* [&] *These authors contributed equally to this work. *Correspondence and requests for materials should be addressed to H.L.L. (email: honglianglu@fudan.edu.cn) or to D. W.Z. (email: dwzhang@fudan.edu.cn).*

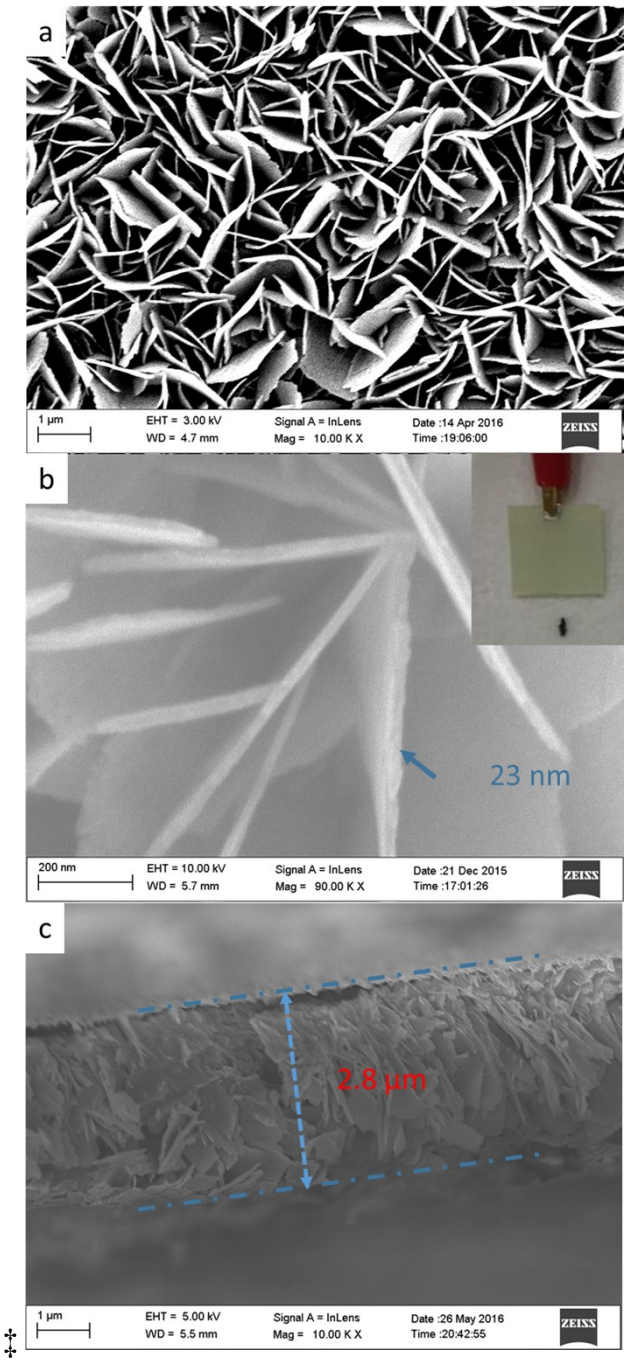

Figure S1. SEM images of as-obtained pure WO_3 nanosheets sample W@T0: (a) Low-magnification and (b) high-magnification top-view images, and (c) a cross section image. Inset in b is the digital photograph of sample W@T0.

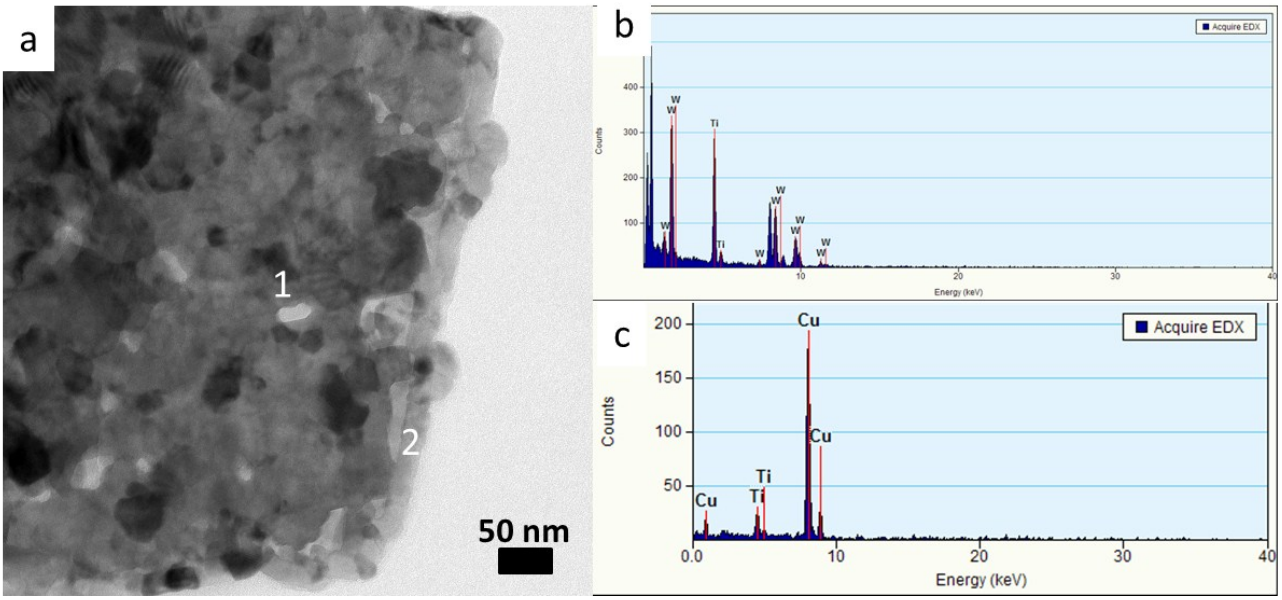

Figure S2. (a) Representative TEM image of the WO_3@TiO_2 core-shell nanosheets with 300 cycles of ALD of the TiO_2 shell (*i.e.* sample W@T15) and the EDS spectra collected correspondingly from (b) Position 1 (*i.e.* the core region) and (c) Position 2 (*i.e.* the shell region).

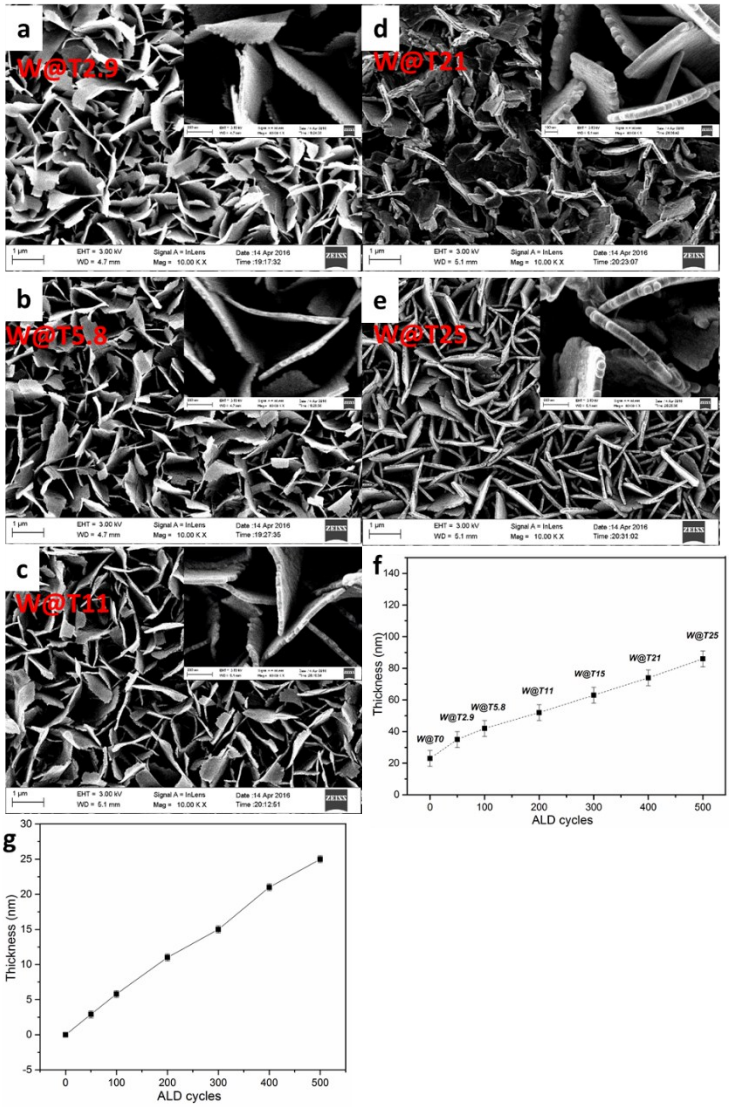

Figure S3. (a–e) Low-magnification SEM images of the obtained WO_3@TiO_2 core-shell nanosheets sample W@T2.9 (a), W@T5.8 (b), W@T11 (c), W@T21 (d) and W@T25 (e); (f) The ALD cycles-dependent increase of the average thickness of the WO_3@TiO_2 core-shell nanosheets; (g) the thicknesses of the TiO_2 layers grown on flat silicon wafers were also measured by llispectroscopic epsometry (SE) and thdetermined from e model-based regression after ALD reaction. Inserts in panel a–e are corresponding high-magnification SEM images of the obtained WO_3@TiO_2 core-shell nanosheets.

As a result, the thicknesses of TiO2 turned out to be 2.9, 5.8, 11, 15, 21 and 25 nm with different ALD cycle numbers of 50, 100, 200, 300, 400 and 500 on flat silicon wafers, by which the average growth rate of the TiO2 layer could be estimated to be ~ 0.5 Å per cycle.

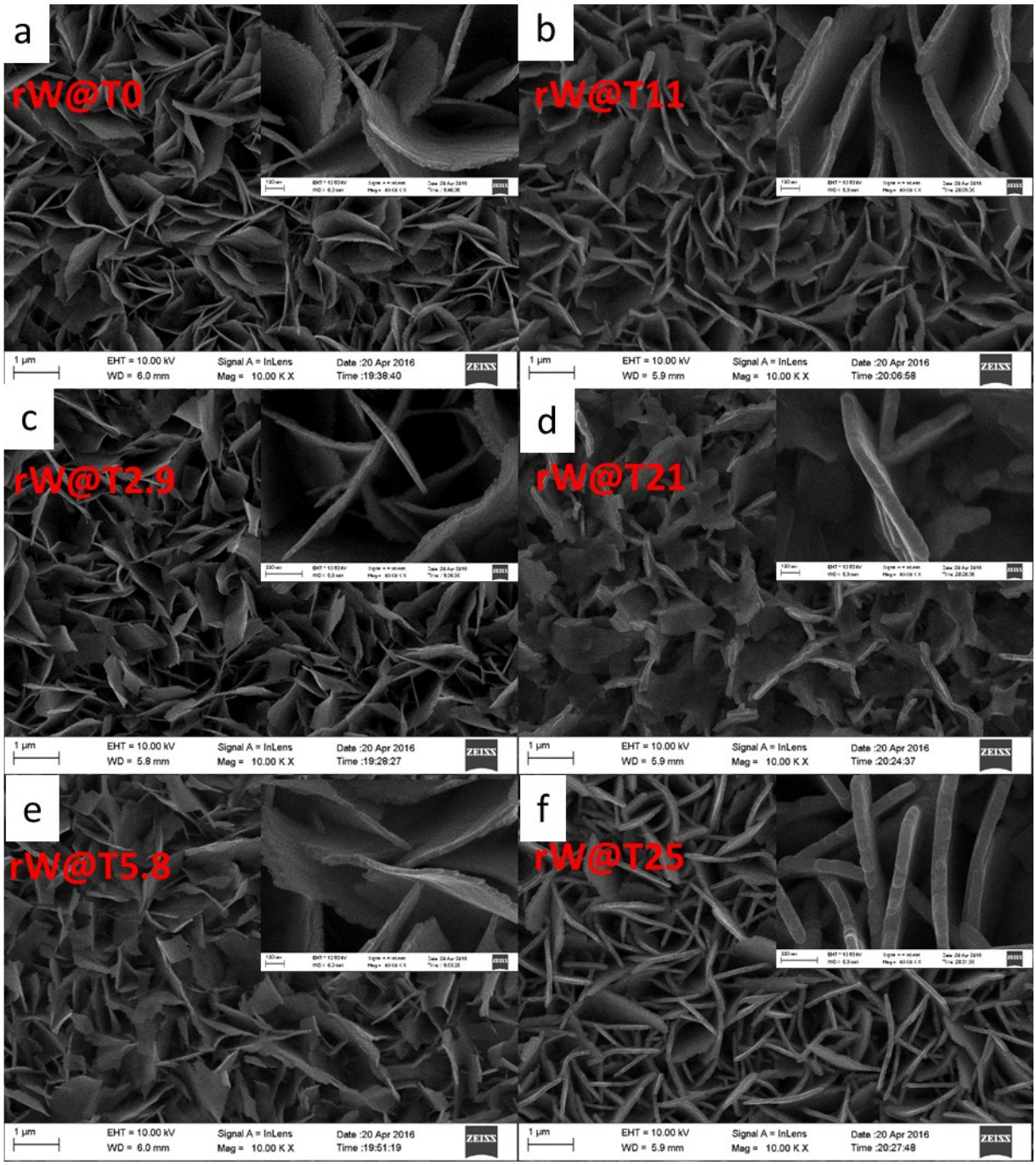

Figure S4. Top-view SEM images of the obtained WO_{3-x}@TiO_{2-x} core-shell nanosheets sample *r*C-0 (a), *r*C-50 (b), *r*C-100 (c), *r*C-200 (d), *r*C-400 (e) and *r*C-500 (f). Inserts in panel a–f are corresponding high-magnification SEM images of these WO_{3-x}@TiO_{2-x} core-shell nanosheets.

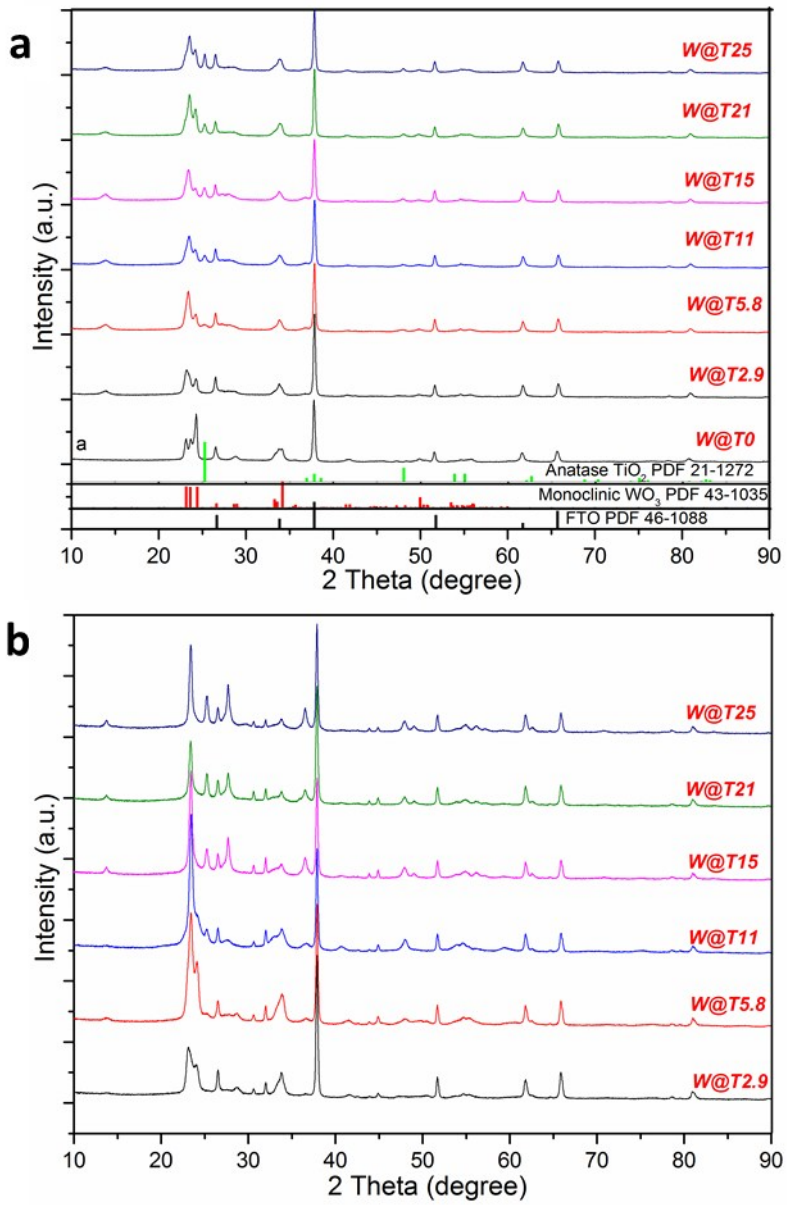

Figure S5. (a) Representative XRD patterns of the synthesized WO_3 and WO_3@TiO_2 nanosheets samples W@T0, W@T2.9, W@T5.8, W@T11, W@T15, W@T21 and W@T25; (b) XRD patterns of the reduced WO_{3-x}@TiO_{2-x} core-shell nanosheets samples *r*W@T2.9, *r*W@T5.8, *r*W@T11, *r*W@T15, *r*W@T21 and *r*W@T25 obtained after H_2 thermal annealing.

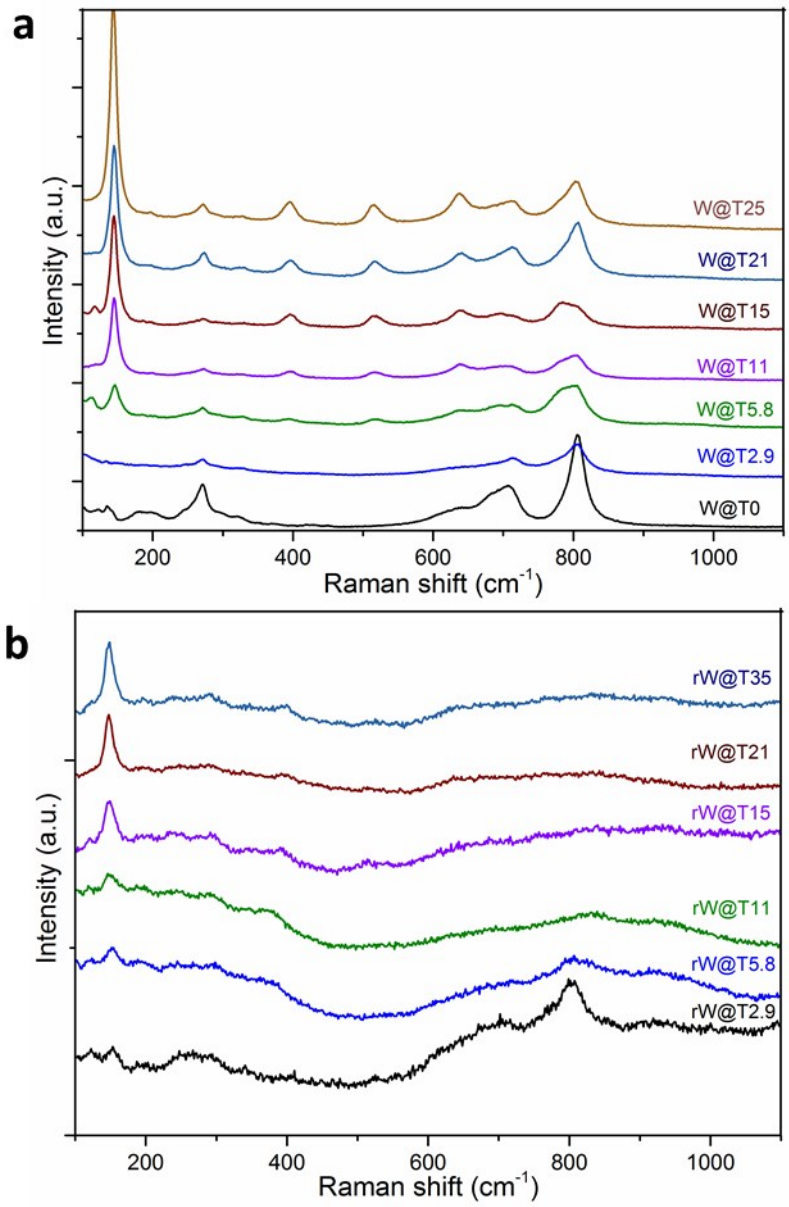

Figure S6. (a) Room-temperature Raman spectra of the WO_3 and WO_3@TiO_2 nanosheets samples W@T0, W@T2.9, W@T5.8, W@T11, W@T15, W@T21 and W@T25; (b) Room-temperature Raman spectra of the reduced WO_{3-x}@TiO_{2-x} core-shell nanosheets samples *rW@T2.9, rW@T5.8, rW@T11, rW@T15, rW@T21 and rW@T25 o*btained after H_2 thermal annealing.

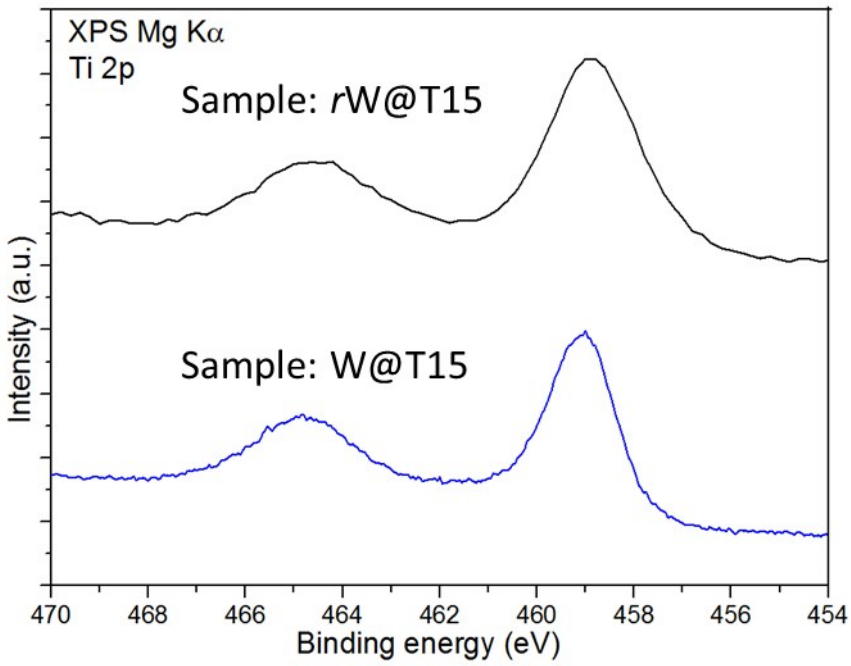

Figure S7. High-resolution Ti 2p XPS spectra of the WO_3@TiO_2 and WO_{3-x}@TiO_{2-x} nanosheets samples W@T15 (blue curve) and *r*W@T15 (black curve).

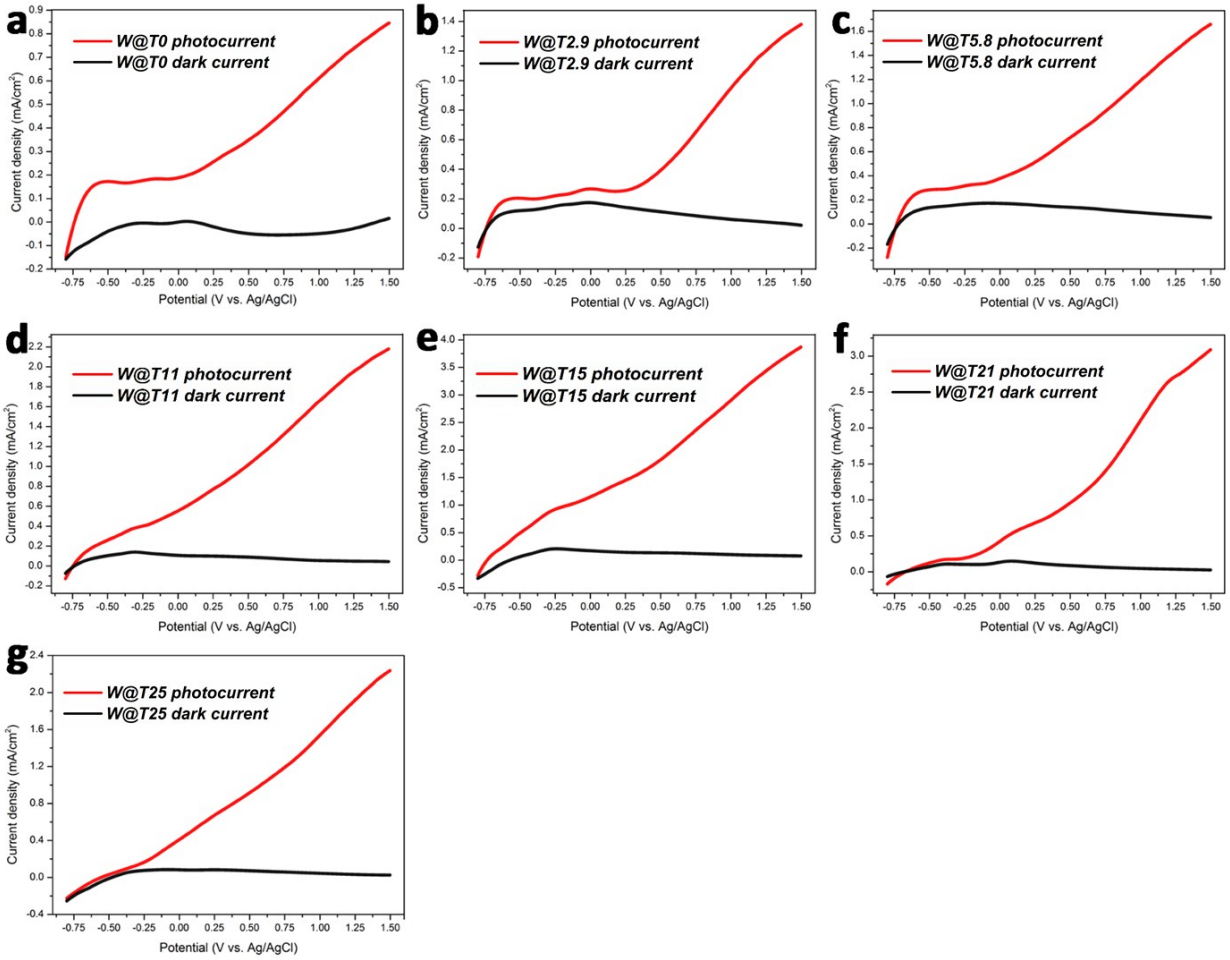

Figure S8. The comparison between the photocurrent (red curves) and dark current densities (black curves) of all the WO_3 and WO_3@TiO_2 nanosheets photoanodes: (a) Sample W@T0, (b) sample W@T2.9, (c) sample W@T5.8, (d) sample W@T11, (e) sample W@T15, (f) sample W@T21 and (g) sample W@T25.

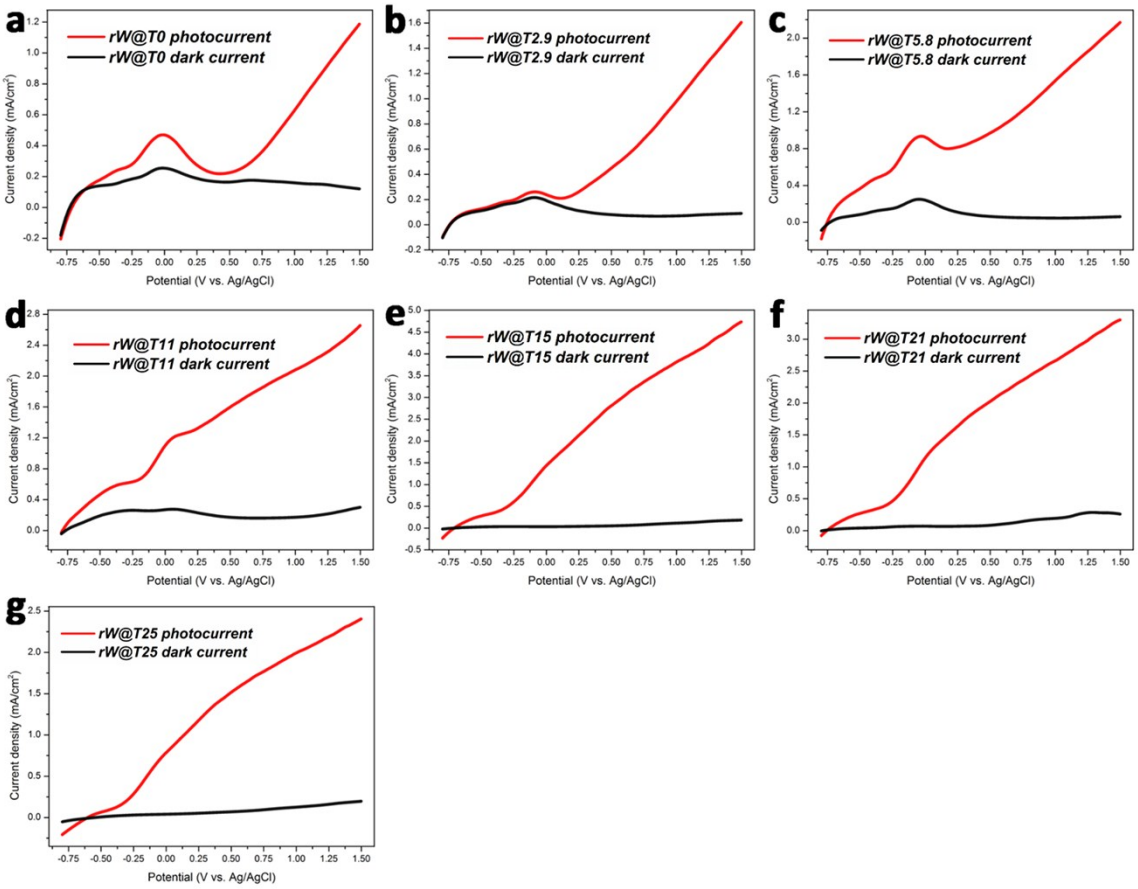

Figure S9. The comparison between the photocurrent (red curves) and dark current densities (black curves) of all the WO_{3-x} and WO_{3-x}@TiO_{2-x} nanosheets photoanodes: (a) Sample *r*W@T0, (b) sample *r*W@T2.9, (c) sample *r*W@T5.8, (d) sample *r*W@T11, (e) sample *r*W@T15, (f) sample *r*W@T21 and (g) sample *r*W@T25.

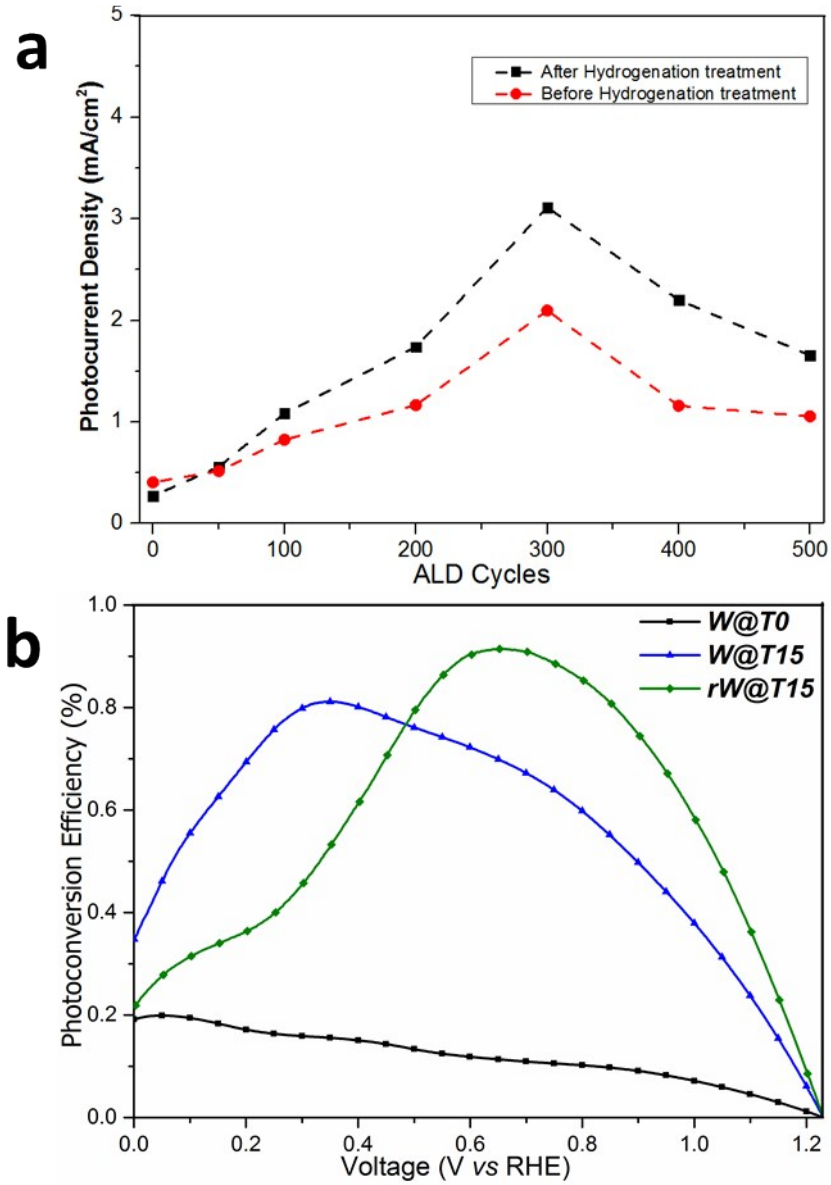

Figure S10. (a) The photocurrent densities of all the obtained WO_3 (*i.e.* sample W@T0), WO_3@TiO_2 (*i.e.* sample W@T2.9, W@T5.8, W@T11, W@T15, W@T21 W@T25), WO_{3-x} (*i.e.* sample *r*W@T0) and WO_{3-x}@TiO_{2-x} (*i.e.* sample *rW@T2.9, rW@T5.8, rW@T11, rW@T15, rW@T21 and rW@T25*) nanosheets photoanodes recorded at 1.23 V vs. RHE; (b) The half-cell solar-to-hydrogen (HC-STH) conversion efficiencies calculated from the LSV curves (Figure 4a–b) of the sample W@T0, W@T15 and *r*W@T15, respectively.

Figure S11. Digital photographs of all the obtained WO_3@TiO_2 and WO_{3-x}@TiO_{2-x} core-shell nanosheets samples.

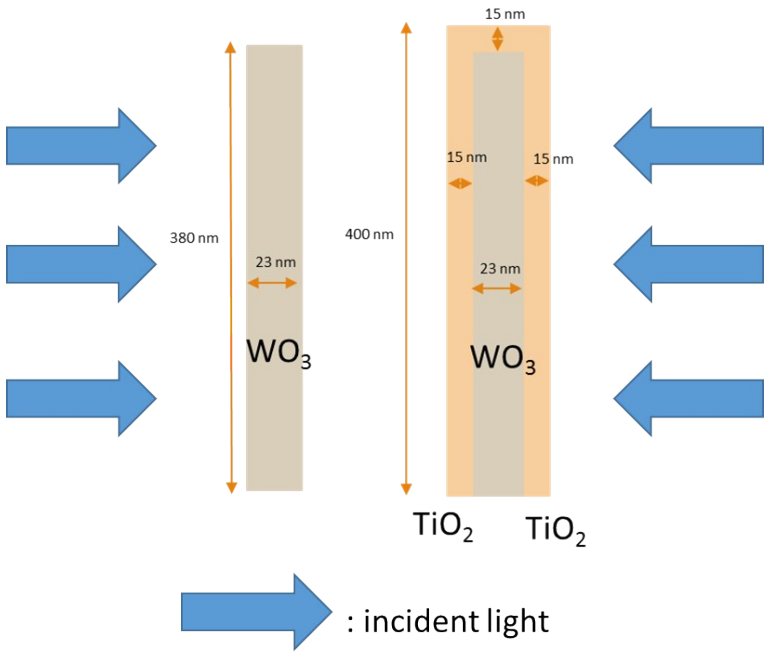

Figure S12. Front view of the FDTD simulation models depicted for the WO_3@TiO_2 core-shell nanosheets sample W@T15 (the right model) and the original pure WO_3 nanosheets sample W@T0 (the left).

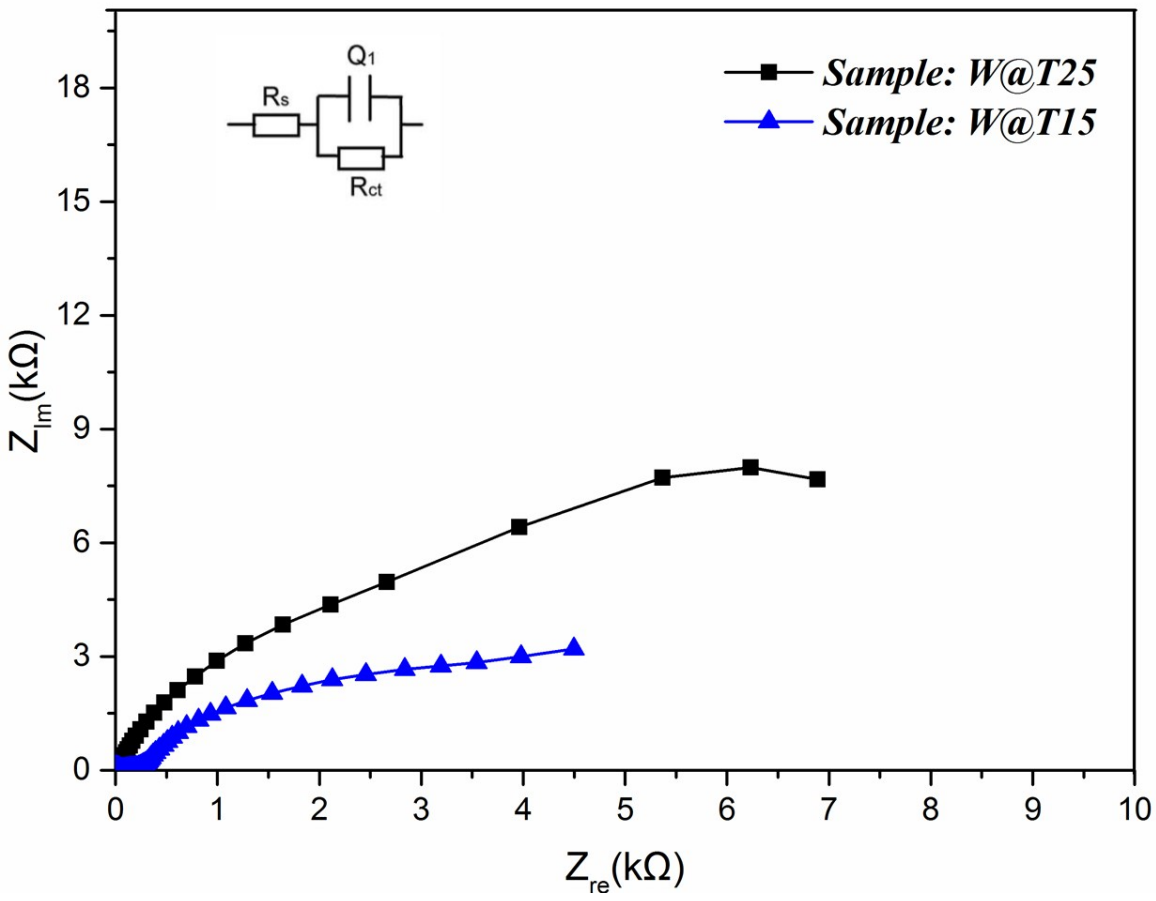

Figure S13. Electrochemical impedance spectroscopy (EIS) Nyquist plots of the obtained WO_3@TiO_2 core-shell nanosheets sample W@T15 (blue curve) and W@T25 (black curve).

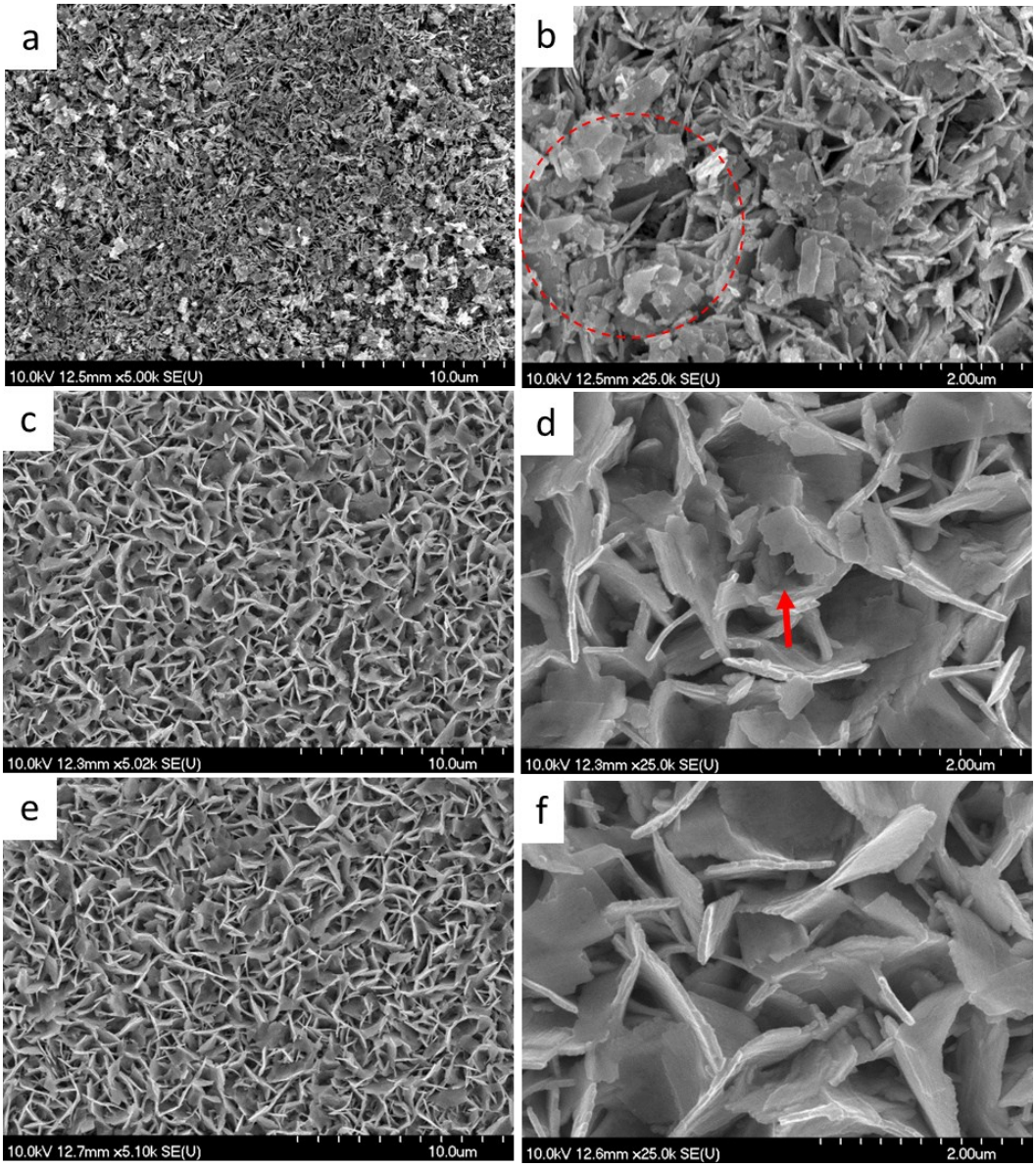

Figure S14. Low-magnification (a, c, e) and high-magnification (b, d, f) SEM images of the photoanodes fabricated from sample W@T0 (a, b), sample W@T15 (c, d) and sample *r*W@T15 after experiencing the 6-h continuous PEC water splitting test.

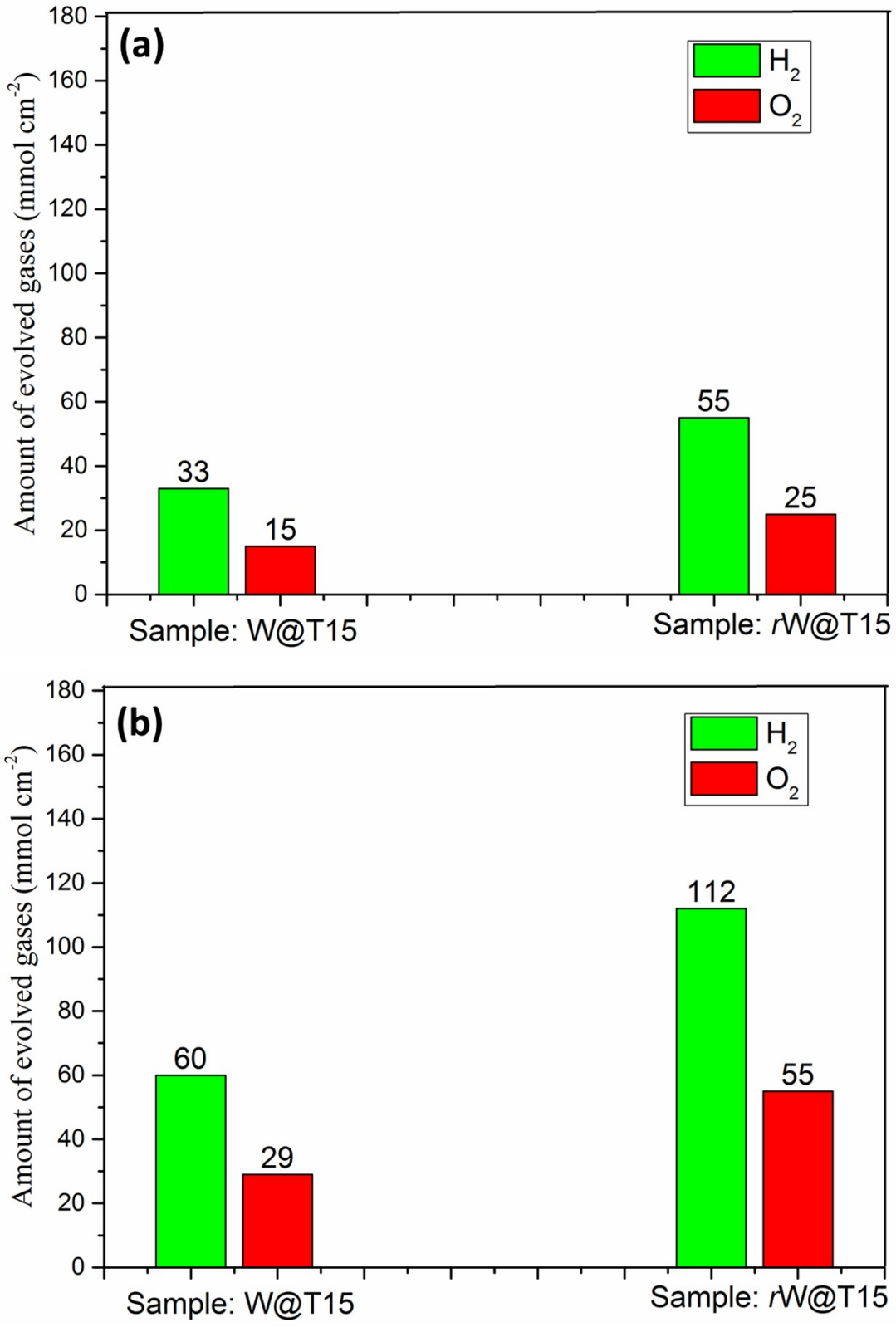

Figure S15. Gas chromatography collection of the oxygen and hydrogen gas evolved from the electrodes after (a) 1-h continuous illumination and (b) 2-h continuous illumination. Specifically during the measurement, the photoanode was biased at 1.23 V vs. RHE.